

# Dust Reverberation Mapping of Type 2 AGN NGC 2110 Realized with X-ray and 3–5 $\mu\text{m}$ IR monitoring

Hirofumi Noda<sup>1,2\*</sup>, Taiki Kawamuro<sup>3</sup>, Mitsuru Kokubo<sup>4</sup>, Takeo Minezaki<sup>5</sup>

<sup>1</sup> Department of Earth and Space Science, Graduate School of Science, Osaka University, 1-1 Machikaneyama, Toyonaka, Osaka 560-0043, Japan

<sup>2</sup> Project Research Center for Fundamental Sciences, Osaka University, 1-1 Machikaneyama, Toyonaka, Osaka 560-0043, Japan

<sup>3</sup> National Astronomical Observatory of Japan, Osawa, Mitaka, Tokyo 181-8588, Japan

<sup>4</sup> Astronomical Institute, Tohoku University, 6-3 Aramaki-zaaoba, Aoba-ku, Sendai, Miyagi 980-8578, Japan

<sup>5</sup> Institute of Astronomy, School of Science, the University of Tokyo, 2-21-1 Osawa, Mitaka, Tokyo 181-0015, Japan

Accepted 2020 May 13. Received 2020 April 19; in original form 2019 September 29

## ABSTRACT

The dust reverberation mapping is one of powerful methods to investigate the structure of the dusty tori in AGNs, and it has been performed on more than a hundred type 1 AGNs. However, no clear results have been reported on type 2 AGNs because their strong optical–UV extinction completely hides their accretion disc emission. Here we focus on an X-ray-bright type 2 AGN, NGC 2110, and utilize 2–20 keV X-ray variation monitored by *MAXI* to trace disc emission, instead of optical–UV variation. Comparing it with light curves in the *WISE* infrared (IR) W1 band ( $\lambda = 3.4 \mu\text{m}$ ) and W2 band ( $\lambda = 4.6 \mu\text{m}$ ) with cross-correlation analyses, we found candidates of the dust reverberation time lag at  $\sim 60$  days,  $\sim 130$  days, and  $\sim 1250$  days between the X-ray flux variation and those of the IR bands. By examining the best-fitting X-ray and IR light curves with the derived time lags, we found that the time lag of  $\sim 130$  days is most favoured. With this time lag, the relation between the time lag and luminosity of NGC 2110 is consistent with those in type 1 AGNs, suggesting that the dust reverberation in NGC 2110 mainly originates in hot dust in the torus innermost region, the same as in type 1 AGNs. As demonstrated by the present study, X-ray and IR simultaneous monitoring can be a promising tool to perform the dust reverberation mapping on type 2 AGNs.

**Key words:** galaxies: active – galaxies: individual (NGC 2110) – galaxies: Seyfert – X-rays: galaxies

## 1 INTRODUCTION

The dusty torus is an important structure in the active galactic nucleus (AGN) and is believed to surround an accretion disc, which lies in the immediate vicinity of the central supermassive black hole (SMBH), and a broad line region (BLR). According to the classical AGN unified model (e.g., Antonucci 1993; Urry & Padovani 1995), all AGNs have the same structure, but appear differently depending on the viewing angle (the angle of the line of sight against the rotation axis of the torus), which determines the differences between the observational classification of the two types of AGNs, types 1 and 2. The AGNs that show optical broad emission lines with a velocity width of  $\gtrsim 2000 \text{ km s}^{-1}$  are classified as type 1, whereas those do not are as type 2. The unified model explains that their viewing angles are different so that the accretion disc and BLR are obscured in the

latter but not in the former. AGN dust tori have been usually studied through analyses of their infrared (IR) spectral energy distributions (SEDs), along with theories developed to explain them. According to the most recent models of the dust torus, the IR continuum emission has multiple emission components, as opposed to a single component, which was once assumed according to the conventional models. The near infrared (NIR) continuum emission, which presumably originates from hot dust residing in the torus innermost region, is now considered to be a separate emission component, and hence, the geometry of the torus innermost region and its relation to neighboring AGN structures such as the accretion disc and the BLR are under much debate (e.g., Mor et al. 2009; Lyu, Rieke & Shi 2017; Hönig & Kishimoto 2017; Baskin & Laor 2018).

The dust reverberation mapping is one of the most powerful tools to investigate the compact structure of the torus innermost region of type 1 AGNs and has been applied to various of them since 1970s (e.g., Penston et al.

\* E-mail: noda@ess.sci.osaka-u.ac.jp

1974; Lebofsky & Rieke 1980; Clavel et al. 1989). When the accretion-disc continuum flux in the optical to ultraviolet (UV) bands varies, the flux of the innermost region of the torus in NIR band responds with dust reverberation time lags  $\tau_{\text{dust}}$ , with which the distance, i.e. radius, from the SMBH to the torus innermost-region can be estimated as  $R_{\text{dust}} = c\tau_{\text{dust}}$ . Since  $R_{\text{dust}}$  is considered to be close to the radius where it is at the dust sublimation temperature of 1700–2000 K (for graphite grains: Huffman 1977; Salpeter 1977; Baskin & Laor 2018),  $R_{\text{dust}}$  is expected to be proportional to the square-root of the disc luminosity,  $R_{\text{dust}} \propto L_{\text{disc}}^{0.5}$  (Barvainis 1987). Large systematic dust-reverberation surveys for type 1 AGNs indeed demonstrated that the dust-reverberation radius approximately follows the radius-luminosity relation of  $R_{\text{dust}} \propto L_{\text{disc}}^{0.5}$  for a wide luminosity range (Suganuma et al. 2006; Koshida et al. 2014; Lyu et al. 2019; Minezaki et al. 2019). Recent advancements of NIR interferometers directly revealed the extent of the innermost dust torus and confirmed its luminosity dependency (e.g., Kishimoto et al. 2011; GRAVITY Collaboration 2019).

However, no clear results of the dust reverberation mappings have been reported about type-2 sources, which dominate the population of AGNs, mainly because their optical/UV emission is heavily or even totally absorbed, rendering monitoring their disc-flux variation difficult or even impossible at the optical or UV wavelengths. A potential way to circumvent this problem with type 2 AGNs is to observe X-rays from a corona lying at an inner part of the accretion disc near the central SMBH as a tracer of disc-flux variation, instead of optical or UV light. Long-term X-ray variation of AGNs is known to show a good correlation with optical/UV variation with a time lag of hours to days for optical/UV lights behind X-rays, as revealed by X-ray and optical/UV monitoring on various type-1 AGNs (e.g., Shappee et al. 2014; Noda et al. 2016). The correlation between the optical/UV and X-rays can be more or less explained as disc reverberation by X-ray irradiation from a corona to the disc (e.g., Krolik et al. 1991; Edelson et al. 2015; Noda et al. 2016). Given that the disc-reverberation time lag between X-rays and optical/UV is negligible compared with  $\tau_{\text{dust}}$ , precise estimate of  $\tau_{\text{dust}}$  with X-ray and NIR monitoring should be feasible. Therefore, we expect that simultaneous X-ray and NIR monitoring observations enable us to realize the dust reverberation mapping of type 2 AGNs for the first time.

In the present paper, we analyze 2–20 keV monitoring data with Monitor of All-sky X-ray Image (*MAXI*; Matsuoka et al. 2009) and the W1 (3.4  $\mu\text{m}$ ) and W2 (4.6  $\mu\text{m}$ ) band photometry data with Wide-field Infrared Survey Explorer (*WISE*; Wright et al. 2010) on the type 2 AGN NGC 2110 (R.A.=5<sup>h</sup> 52<sup>m</sup> 11.4<sup>s</sup>, Dec.=−7<sup>d</sup> 27<sup>m</sup> 22<sup>s</sup>), which is well known and X-ray bright (Kawamuro et al. 2018). NGC 2110 is a nearby Compton-thin type-2 Seyfert galaxy with a redshift of 0.0078 at a distance of 31.2 Mpc (Storchi-Bergmann et al. 1999). Two independent measurements of the mass of the SMBH at its centre were reported; Woo & Urry (2002) showed  $M_{\text{BH}} = 2.0 \times 10^8 M_{\odot}$ , using the relation between  $M_{\text{BH}}$  and stellar velocity dispersion, whereas Minezaki & Matsushita (2015) reported  $M_{\text{BH}} = 2.5 \times 10^7 M_{\odot}$ , using the velocity width of the narrow Fe-K $\alpha$  line. We adopt cosmological parameters of  $H_0 = 73 \text{ km s}^{-1} \text{ Mpc}^{-1}$ ,  $\Omega_{\Lambda} = 0.73$ , and  $\Omega_{\text{m}} = 0.27$  throughout this

paper. Errors shown in text and figures refer to those in 1 $\sigma$  confidence, unless otherwise stated.

## 2 OBSERVATIONS AND DATA REDUCTION

### 2.1 X-ray data

*MAXI* onboard the International Space Station (ISS) has been operated from 2009 August 15, continuously monitoring all sky with the Gas Slit Cameras (GSCs; Mihara et al. 2011) in 2–30 keV and the Solid-state Slit Cameras (SSC; Tomida et al. 2011) in 0.5–12 keV. Since soft X-rays of NGC 2110 are heavily absorbed by the torus (Kawamuro et al. 2016), we use hard X-ray data above 2 keV obtained by the GSCs only in this work. The GSCs cover two 84°-separated regions with fields of view of 3° × 160° and observe individual areas of the sky every 92 minutes synchronized with the rotation of the ISS. The GSCs can observe 85% and 95% of all sky per one ISS rotation and one day respectively. Thus NGC 2110 has been monitored almost everyday.

Using the on-demand pipeline provided by the *MAXI* team (<http://maxi.riken.jp/mxondem/>), we reduced the GSC data of NGC 2110 obtained from 55000 to 58500 MJD and extracted a 30-days binned light curve in the 2–20 keV band. We also extracted 60-days binned light curves in the 2–6 keV and 6–20 keV bands and made a curve of a hardness ratio of the 6–20 keV to 2–6 keV fluxes, using the default on-demand interface.

### 2.2 3–5 $\mu\text{m}$ IR data

*WISE* is an astronomical infrared satellite, launched on 2009 December 14, and performed all-sky survey until 2011 at the 3.4, 4.6, 12, and 22  $\mu\text{m}$  bands named W1, W2, W3, and W4, respectively. The programme *Near-Earth Objects WISE* (*NEOWISE*) (Mainzer et al. 2014) started in 2013 after the initial and primary programme with use of cryogen and has been running since then, after a long period of interruption from 2011 February to 2013.

In this work, we used the *AllWISE* multi-epoch photometry table and *NEOWISE* single exposure (L1b) source table fetched from the NASA/IPAC Infrared Science Archive (<https://irsa.ipac.caltech.edu/Missions/wise.html>). We obtained the photometry results in an area within a 10'' radius of (RA, Dec) = (88.04742, −7.45621) in the J2000 coordinates, and took the values of the W1 magnitude `w1mpro_ep`, W1 magnitude error `w1sigmpro_ep`, W2 magnitude `w2mpro_ep`, W2 magnitude error `w2sigmpro_ep`, and MJD `mjd`. The *WISE* magnitude values were converted to the flux density  $F_{\nu}$  according to the equation  $F_{\nu} = F_{\nu,0} \times 10^{(-m/2.5)}$ , where  $F_{\nu,0} = 309.540 \text{ Jy}$  and  $171.787 \text{ Jy}$  for the W1 and W2 bands, respectively, and  $m$  is the *WISE* magnitude. After the conversions, the averages of the flux densities per visit were calculated and accepted as the W1 and W2 fluxes in each visit.

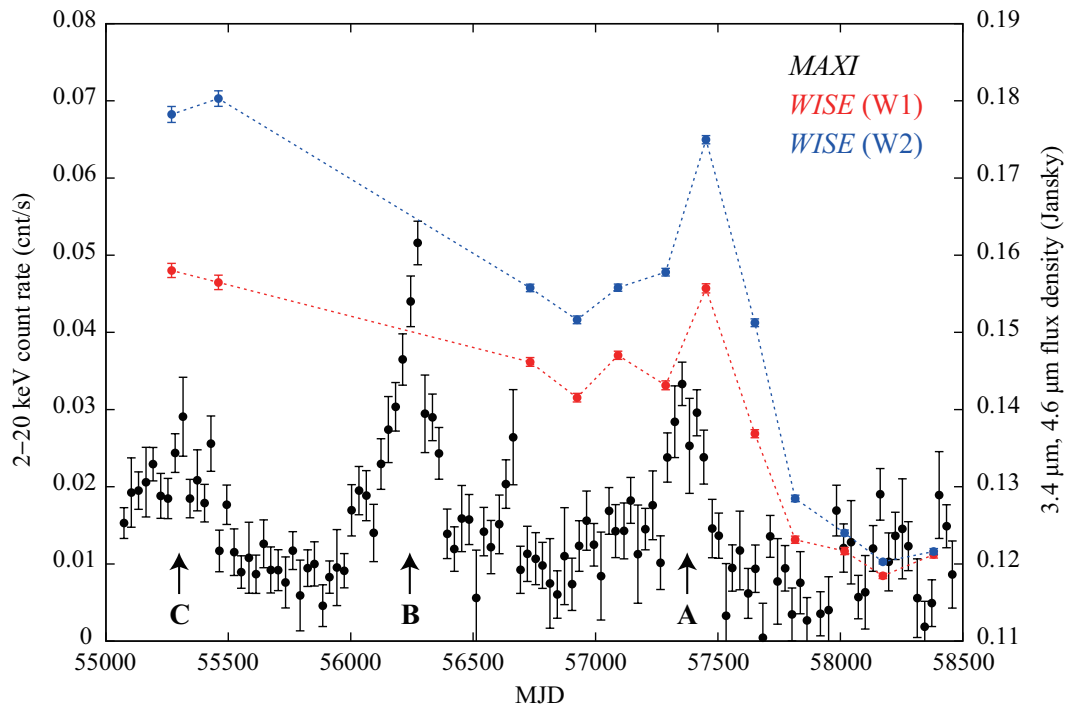


**Figure 1.** Light curves in (black) 2–20 keV with *MAXI*/GSC and the (red) W1 and (blue) W2 bands with *WISE*. The dotted lines simply connect the W1 and W2 individual data points. The X-ray flares at 57250–57500 MJD, 56000–56500 MJD and 55000–55500 MJD are named peaks A, B and C, respectively.

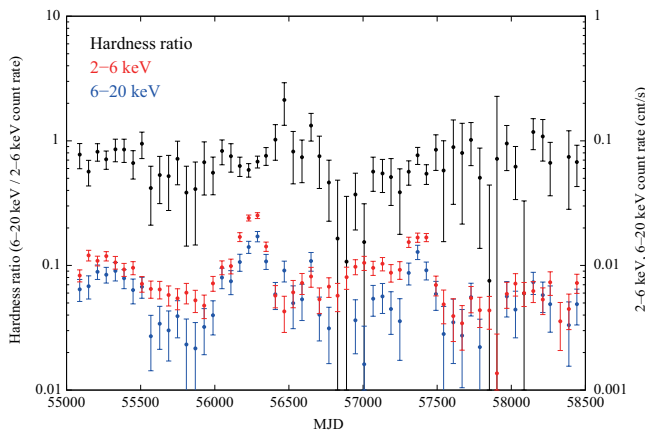


**Figure 2.** Light curves in the (red) 2–6 keV and (blue) 6–20 keV bands, and a curve of (black) their ratio (hardness ratio).

### 3 DATA ANALYSIS

#### 3.1 X-ray and 3–5 μm flux correlation with dust-reverberation time lag

Figure 1 shows long-term light curves in the 2–20 keV band with *MAXI* and in the W1 and W2 bands with *WISE*. A significant variation in the 2–20 keV band was detected with an unprecedentedly high-cadence observations with *MAXI*. The most remarkable was three distinctive flares at 57250–57500 MJD, 56000–56500 MJD, and 55000–55500 MJD from later to earlier; hereafter we refer to them as the (X-ray) peaks A, B, and C, respectively, as marked in Fig. 1. The

2–20 keV flux varied by a factor of  $\sim 3$  and  $\sim 5$  in peaks A and B, respectively, each lasting hundreds of days.

This kind of long-term X-ray flux variation is considered to show a good correlation with that of disc emission in optical/UV band (e.g., Shappee et al. 2014; Noda et al. 2016; Edelson et al. 2017), whereas fast X-ray variation on a timescale of hours–days is known to be uncorrelated to optical/UV variation (e.g., Gardner & Done 2017; Edelson et al. 2017)<sup>1</sup>. The bin size of the *MAXI* light curve of  $\sim 1$  month in Fig. 1 is long enough to smear out fast X-ray variability to represent the long-term X-ray flux variation, and hence, the X-ray light curve can be used as a tracer of the disc flux variation of NGC 2110.

Since NGC 2110 is a type 2 AGN, its X-ray flux could be highly variable when a column density of the obscurers changes. In order to examine whether the variability is intrinsic or originates from the column density change, we made light curves in the 2–6 keV and 6–20 keV band, and produced a curve of the hardness ratio between them as shown in Fig. 2. Then we performed a fit to the curve of the hardness ratio with a constant function to examine whether

<sup>1</sup> Edelson et al. (2017) suggested that X-ray flux variation on a timescale of months is correlated with optical/UV flux variation because of reprocess by the warm disc emitting soft X-rays, which is observed as a soft X-ray excess component (e.g., Mehdipour et al. 2011; Noda et al. 2011; 2013; Petrucci et al. 2018; Noda & Done 2018). As an alternative suggestion, Noda et al. (2016) discussed that an additional rapidly-varying X-ray component (Noda et al. 2011; 2013; 2014; Miyake et al. 2016) appears or disappears, affecting the X-ray–optical/UV correlation.

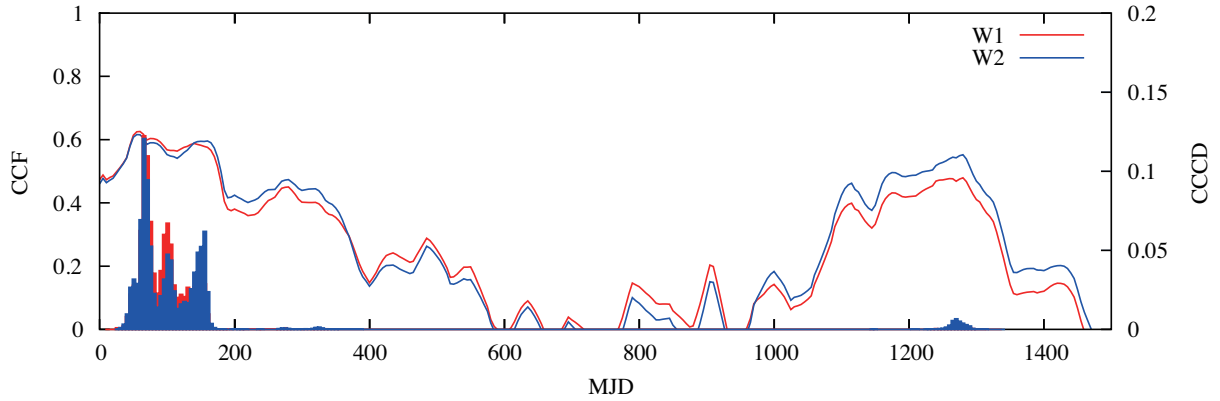


**Figure 3.** ICCFs between the 2–20 keV and the (red) W1 and (blue) W2 bands data, along with the histogram of their CCCD.

the hardness had variability or not and found an acceptable fit of  $\chi^2/\text{d.o.f.}=63.1/57$ . This shows that the variation of the hardness ratio was not significant, and hence the X-ray variations were not mainly because of a potential variation of the absorption column density.

Figure 1 also shows the W1- and W2-band light curves. The period of peak A was covered by the *NEOWISE* phase with intervals of  $\sim 180$  days, whereas neither of them covered the period of 55500–56500 MJD around peak B. A flare was detected at around 57500 MJD, roughly coinciding with X-ray peak A. The amplitude of the IR flare was  $\sim 10\%$  in both the W1- and W2- bands. In the following analyses, we examine the significances of the IR flare responses to X-ray peaks A and B. Peak C is not considered in this analysis, because the total length of the monitoring period is so limited that the correlations between the delayed X-ray light curves with delays of  $\gtrsim 2000$  days and the IR light curves are difficult to be examined, where the number of the available data points would be too small for the correlation analysis to be statistically meaningful.

In order to study the correlations between X-ray and the NIR flux variations, we conducted analysis of the interpolation cross correlation function (ICCF; Peterson et al. 1998) with a time lag ( $\tau$ ) range of 0–1500 days. In the ICCF analysis, the interpolation was applied to only the X-ray light curve with the time step of 5 days, because the X-ray sampling was dense enough for the interpolation whereas the IR samplings were sparse. In order to estimate the error of the time lags, the flux randomization method was employed with 30000 realizations in the Monte Carlo simulations<sup>2</sup>.

Figure 3 shows ICCF curves and cross correlation centroid distributions (CCCDs) derived with the ICCF analysis. Significant time lags  $\tau$  in the W1 band ( $\tau_{W1}$ ) and W2 band ( $\tau_{W2}$ ) were obtained to be  $\sim 60$ –150 days for both at 5% significance level (correlation coefficients are  $\sim 0.60$  with  $n = 12$ ). This corresponds to the IR response to X-ray peak A. The correlation coefficients were  $\sim 0.47$  ( $n = 12$ ) at  $\tau_{W1} = 0$  and  $\sim 0.46$  ( $n = 12$ ) at  $\tau_{W2} = 0$  days, implying that the correlation with no time lag was not significant at 5% significance level. Another CCF peak was found at  $\tau \sim 1250$  days for both, which corresponds to the IR response to X-ray peak B. However,  $\tau_{W1} \sim 1250$  days was not significant even at

10% significance level, whereas  $\tau_{W2} \sim 1250$  days was significant at the same significance level, from their correlation coefficients.

In order to further examine the time lags obtained with the ICCF analysis, we employed the JAVELIN algorithm (Zu et al. 2011; Zu et al. 2013). The JAVELIN technique assumes a primary light curve to follow the dumped random walk (DRW) process (e.g., Kelly et al. 2009) and convolves it with a top-hat transfer function (TF) to make a responding light curve, searching with the Markov chain Monte Carlo (MCMC) method for the most likely values for the following five parameter: the amplitude and timescale of the DRW process, height and width of the top-hat TF, and response time delay. In our analysis, we assigned the 2–20 keV light curve, which has a much higher cadence than the IR ones, as the primary variation, and the W1- and W2-band light curves as the responding variation.

First, we restricted the  $\tau$  range to be 0–1500 days, which is the same as that in the ICCF analysis, while no restriction was applied to the width ( $w$ ) range of the top-hat TF. Top panel in Fig. 4 shows the results of the JAVELIN simulations. Similar to the results of the ICCF analysis in Fig. 3, multiple likelihood peaks were found at time lags (both  $\tau_{W1}$  and  $\tau_{W2}$ ) of  $\sim 60$  days,  $\sim 130$  days, and  $\sim 1250$  days. Furthermore, we obtained likelihood peaks of  $w \sim 0$  days and 300–350 days (inset of the top panel of Fig. 4).

Then, in order to identify the  $\tau$  peaks corresponding to  $w \sim 0$  days and  $w \sim 300$ –350 days separately, we performed the JAVELIN simulations where the  $w$  range was restricted to be 0–100 days and 200–400 days, respectively. The middle and bottom panels of Fig. 4 show the resultant respective likelihood distributions. We found three peaks in the likelihood distributions of  $\tau_{W1}$  and  $\tau_{W2}$  for  $w = 0$ –100 days ( $\tau \sim 60, 140, 1280$  days), whereas two peaks for  $w = 200$ –400 days ( $\tau \sim 130, 1230$  days). No significant differences between  $\tau_{W1}$  and  $\tau_{W2}$  were found. Table 1 lists the resultant  $\tau_{W1}$  and  $\tau_{W2}$  and their  $1\sigma$  errors. The insets of the middle and bottom panels of Fig. 4 show the likelihood distributions of the widths of the top-hat TF in the W1 band ( $w_{W1}$ ) and W2 band ( $w_{W2}$ ). Their values were estimated to be  $8.2^{+16.7}_{-6.3}$  and  $9.4^{+20.4}_{-7.3}$  days for  $w_{W1}$  and  $w_{W2}$ , respectively, for  $w = 0$ –100 days, and similarly  $302.6^{+17.8}_{-26.9}$  and  $326.9^{+13.8}_{-20.9}$  days, respectively, for  $w = 200$ –400 days.

<sup>2</sup> We used the code pyCCF in <http://ascl.net/code/v/1868>



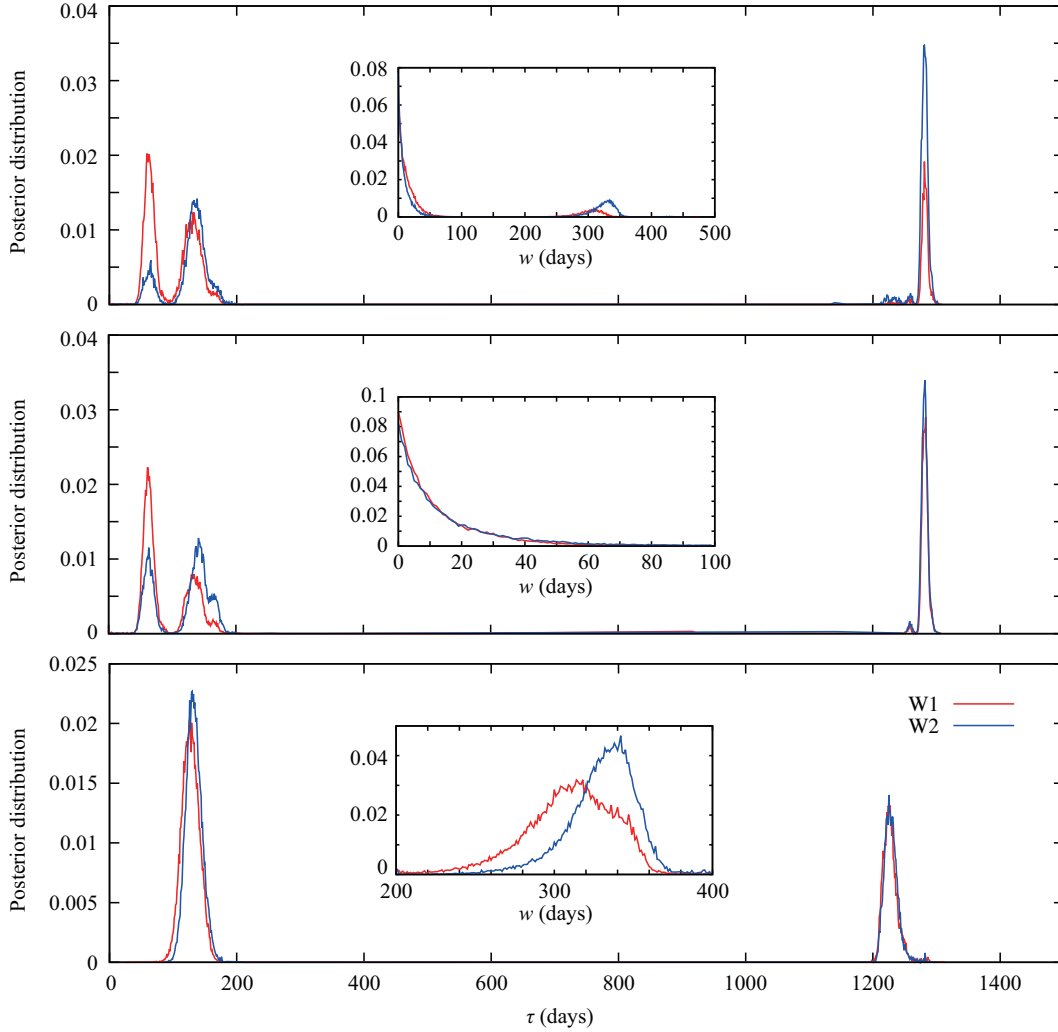


**Figure 4.** (top) Posterior distributions of  $\tau$  in the W1 (red) and W2 (blue) bands behind the 2–20 keV emission obtained with the JAVELIN algorithm without limiting  $w$ . Inset in each panel shows posterior distributions of  $w$  derived with the same JAVELIN run. (middle) Same as top panel, but by restricting  $w$  within 0–100 days. (bottom) Same as top panel, but by restricting  $w$  within 200–400 days.

**Table 1.** Detected  $\tau$  of the W1 and W2 bands behind the X-ray data measured with the JAVELIN simulations. Errors refer to  $1\sigma$  uncertainties.

$w$ range (days)	$\tau_{W1}$ (days)	$\tau_{W2}$ (days)
0–100	$63.3^{+8.8}_{-8.1}$	$63.5^{+9.1}_{-9.2}$
	$135.5^{+15.6}_{-13.4}$	$143.8^{+20.2}_{-14.0}$
	$1281.4^{+4.8}_{-6.3}$	$1281.2^{+5.1}_{-5.6}$
200–400	$127.5^{+14.0}_{-13.7}$	$132.9^{+13.6}_{-11.8}$
	$1226.6^{+11.9}_{-9.3}$	$1228.0^{+10.8}_{-9.2}$

### 3.2 Examining Modelled Light Curves

The JAVELIN simulation calculate the modelled light curve, which is the expected average of all possible light curves, and its uncertainty, which is the variance of them, for both the source (X-ray) and response (IR) flux variations. The next step is to find which likelihood distribution peak of  $(\tau, w)$

is the most favoured from these best-fitting modelled light curves. For this purpose, we performed additional JAVELIN simulations for each likelihood peak of  $\tau$  restricting the  $w$  range within 0–100 days and 200–400 days.

Figure 5(a) and (b) show the modelled light curves for  $(\tau, w) \sim (60, 12)$  and  $(140, 12)$  days, respectively. At first glance, both IR and X-ray modelled light curves well reproduce the observed flux data, including even flux variations on timescales of  $\sim 100$  days. However, a closer look at both the IR modelled light-curves reveals that remarkable flux variations happen in many of the half-year gaps of the observed epochs during  $\sim 57800$ – $58500$  MJD, while none of the observed points (Fig. 1) show much variation. In other words, most of sharp positive peaks conveniently fall between observed epochs. The sharp dip at around  $\sim 57450$  MJD which splits a major peak (corresponding to peak A) in the IR modelled light-curve in Fig. 5(a) upper panels appears rather artificial. In addition, it has been known that the AGN central engine usually shows a smaller flux variation in shorter timescales, and moreover that the IR responses to its short-term flux variations are smeared regardless of the geometry

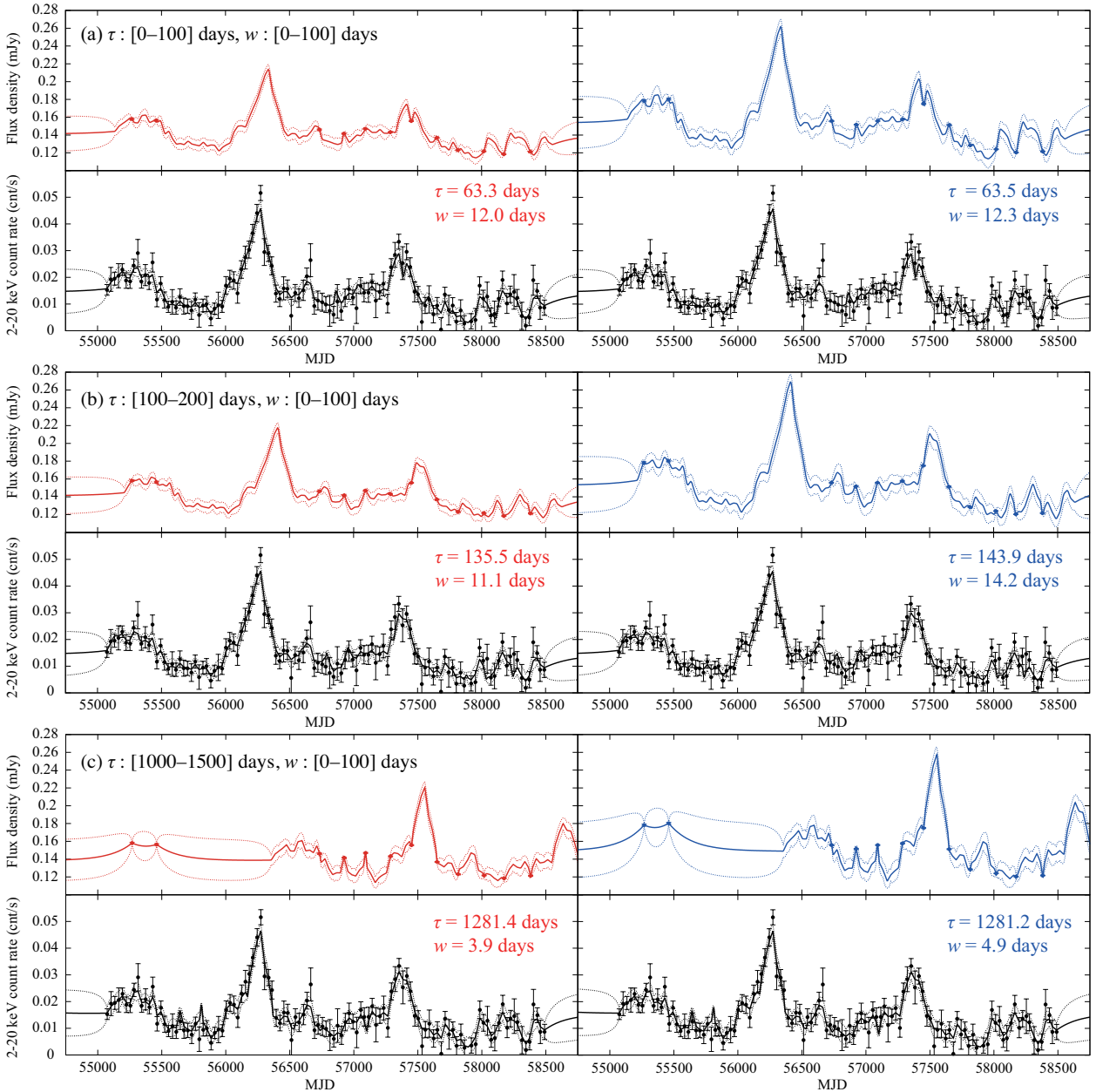
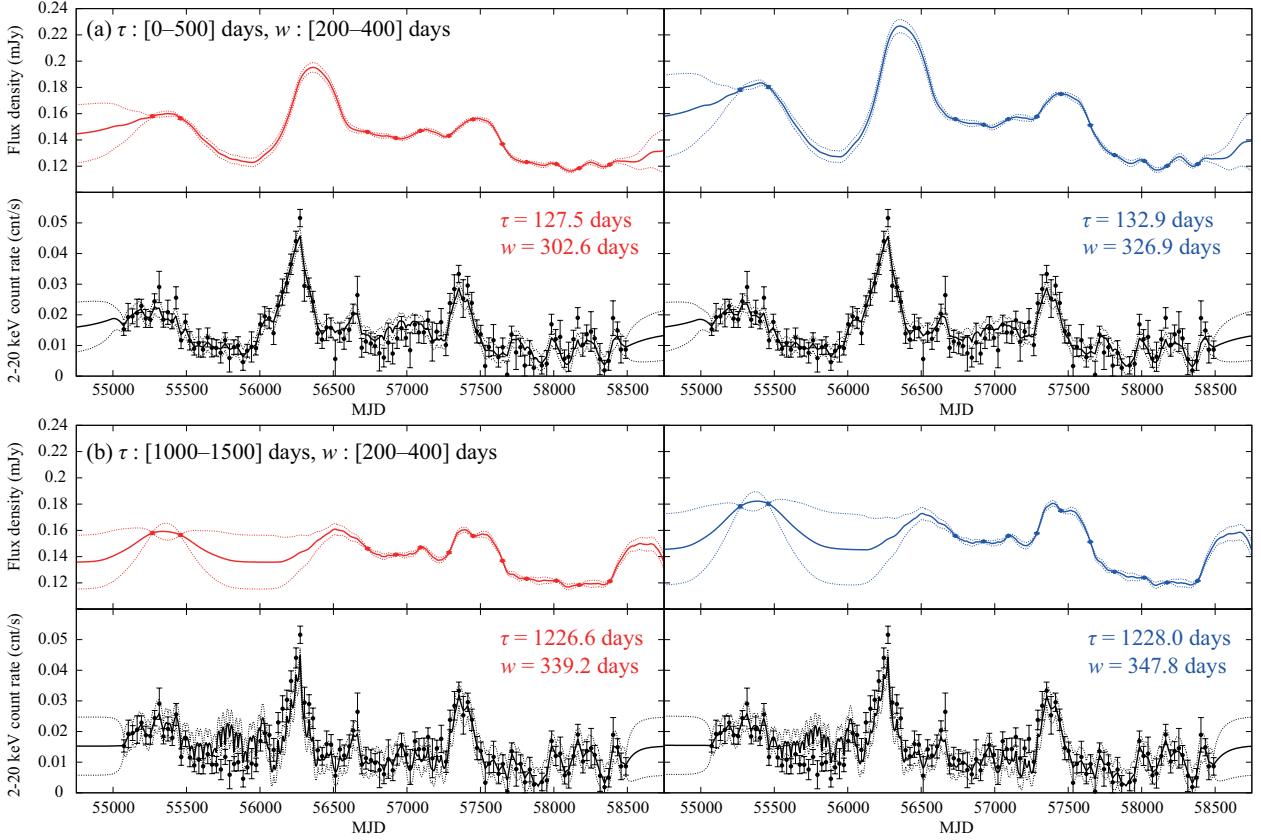


**Figure 5.** Best-fitting interpolated light curves (solid line) and their errors (dotted line) corresponding to the peaks in the top panel of Fig. 4, derived with the JAVELIN runs restricting  $w$  within 0–100 days and  $\tau$  within (a) 0–100 days, (b) 100–200 days, (c) 1000–1500 days. In each set of  $2 \times 2$  panels, top two panels show the best-fitting light curves in the W1 (left panel, in red) and W2 (right panel, in blue) bands, whereas the two bottom panels show those in 2–20 keV simulated with the (left panel) W1 and (right) W2 bands. The best-fitting values of  $\tau$  and  $w$  are shown in each panel in the same colours as the light curves.

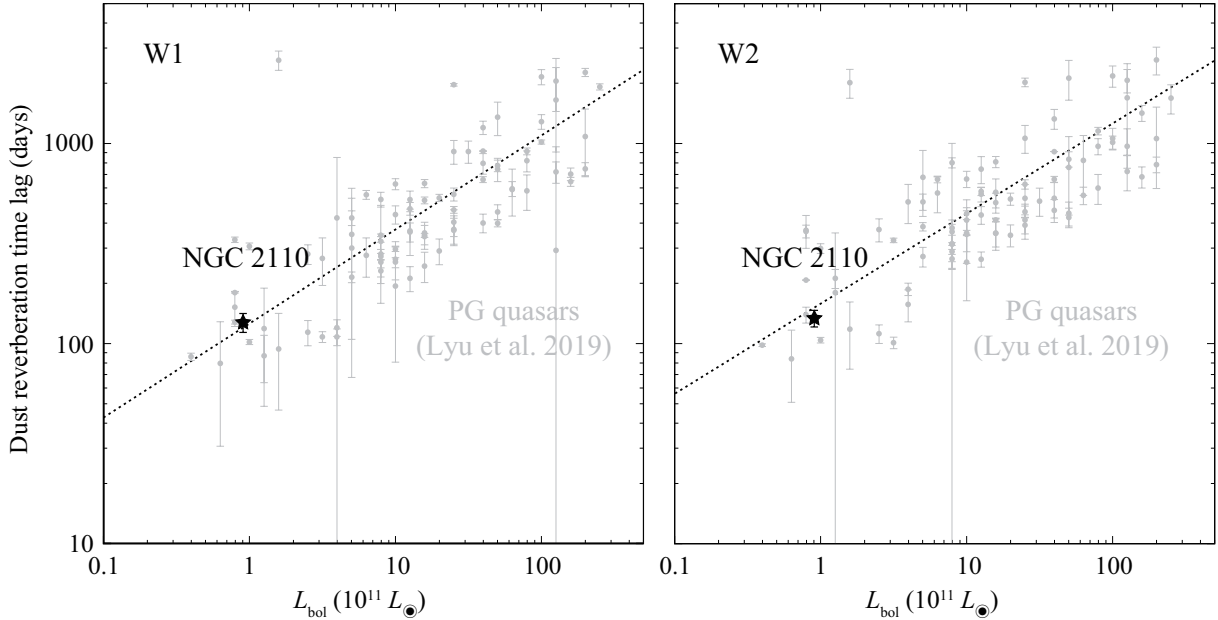
of the IR emitting region unless the viewing angle is perfectly face-on (e.g., Barvainis 1992; Lyu et al. 2019). This fact suggests short-term variations in the IR light-curve as in the modelled light-curves to be even less realistic. Therefore, the remarkable IR flux variations that happens “conveniently” in gaps of the observed epochs in the modelled light-curves are, though one of the mathematical solutions, unlikely to be the real case.

Figure 5(c) shows the modelled light curves for  $(\tau, w) \sim (1280, 12)$  days. In this case, the IR modelled light curves show remarkable flux variations on timescales of less than half a year in not only similar periods of observation gaps

as in the previous two cases but also during  $\sim 56700$ – $57300$  MJD, where again none of the observed points show much variation. We interpreted that the distinctive variation during  $\sim 56700$ – $57300$  MJD, which is characterized with two sharp peaks coinciding at the two observed epochs in each IR band, originated in the mismatch between the IR flux level during the period and the X-ray flux level 1280 days prior to it, i.e. during  $\sim 55400$ – $56000$  MJD. More specifically, since the errors of the observed IR flux data are very small, the IR modelled fluxes at the observing epochs are inevitably constrained to be very close to the observed data, whereas at any other epochs they remain faint, following the X-ray



**Figure 6.** Same as Figure 5 but corresponding to the peaks in the bottom panel of Fig 4 and for (a)  $\tau$  within 0–500 days and  $w$  within 200–400 days, and (b)  $\tau$  within 1000–1500 days and  $w$  within 200–400 days.



**Figure 7.** Left panel shows the correlation between  $\tau_{W1}$  and  $L_{\text{bol}}$  of NGC 2110 and PG quasars from Lyu et al. (2019), whereas right panel shows that between  $\tau_{W2}$  and  $L_{\text{bol}}$ . The black star in each panel shows the data point for NGC 2110 for  $\tau_{W1} \sim \tau_{W2} \sim 130$  days, and grey circles show those of PG quasars. Error bars do not include the uncertainty of the NGC 2110 luminosity due to that of the bolometric correction for the X-ray luminosity.

flux data points. We conclude that these strong short-term flux variations in IR and the sharp peaks in X-rays in the modelled light curves during these epochs are not realistic.

Figures 6(a) and (b) show the modelled light curves for  $(\tau, w) \sim (130, 310)$  and  $(1260, 340)$  days, respectively. In both cases, we found that the IR modelled light curves connected the observed data points smoothly. In the former case ( $(\tau, w) \sim (130, 310)$  days), the X-ray modelled light curves also successfully follow the observed data points overall for the entire observed period. In the latter case ( $(\tau, w) \sim (1260, 340)$  days), however, the X-ray modelled light curves were brighter than the observed data points during  $\sim 55500$ – $56000$  MJD. We interpret that this flux discrepancy was caused by the same origin as for the mismatch between the IR and X-ray flux levels at the corresponding epochs in the case of  $(\tau, w) \sim (1280, 12)$  days (see previous paragraph). In this case, the X-ray flux variations in short timescales were smeared out by the large- $w$  TF and accordingly resulted in the smooth IR modelled light curves. Then, the IR modelled fluxes stayed close to the observed data points, whereas the X-ray modelled fluxes did not, probably because the errors of the IR flux data points were much smaller than those of the X-ray ones.

Finally we conclude that the most favoured parameter set of the dust-reverberation time lags in NGC 2110 are  $\tau_{W1} = 127.5^{+14.0}_{-13.7}$  days and  $\tau_{W2} = 132.9^{+13.6}_{-11.8}$  days with TF widths of  $w_{W1} \sim 300$  days and  $w_{W2} \sim 330$  days (Figure 6a).

### 3.3 Comparison of $\tau$ – $L$ relation with type 1 AGNs

The dust-reverberation radius is known to be correlated well with the AGN luminosity for type 1 Seyfert galaxies and quasars, and its origin is well explained by the dust reverberation at the innermost region of the dusty torus (e.g., Koshida et al. 2014; Minezaki et al. 2019; Lyu et al. 2019). Here we examine whether or not the dust reverberation lags and the luminosity of the type 2 AGN NGC 2110 follow the same trends.

Since we have obtained the dust-reverberation lags for the *WISE* W1 and W2 bands ( $\tau_{W1}$  and  $\tau_{W2}$ ), we compare the correlation between the dust-reverberation lags in the same bands and the bolometric luminosity presented by Lyu et al. (2019). In order to estimate the bolometric luminosity of NGC 2110, we utilize  $L_{14-195 \text{ keV}} \sim 4.3 \times 10^{43} \text{ erg s}^{-1}$  reported by Ricci et al. (2017), and multiply the bolometric correction factor of 8 (Vasudevan & Fabian 2009), following the estimate by Koss et al. (2017). In Fig. 7, we plot the dust-reverberation lags ( $\tau_{W1}$  and  $\tau_{W2}$ ) and  $L_{\text{bol}}$  of NGC 2110 on those of type-1 PG quasars reported by Lyu et al. (2019). The data points of NGC 2110 are found to be located on the best-fitting correlations for the PG quasars. A potential issue that has not been considered is the systematic uncertainty in the bolometric correction, which is reported to be approximately 0.5 dex (Vasudevan & Fabian 2009). Then we find that even if this uncertainty is incorporated, the data points of NGC 2110 are still consistent with the correlation for the PG quasars. This result indicates that the origin of the NIR flux variation of NGC 2110 is the same as in type 1 AGNs; i.e. the NIR emission responsible for the flux variation comes from the innermost region of the dust torus and responds to the flux variation of the central engine with a lag.

## 4 DISCUSSION

We have measured a dust-reverberation lag in a type 2 Seyfert AGN for the first time; the time lag between the X-ray and NIR (continuum emission in the W1 and W2 bands) flux variations of NGC 2110 was estimated to be  $\tau_{\text{dust}} \sim 130$  days. This value is consistent with the dust-reverberation radius-luminosity relation for type 1 AGNs. This fact suggests that the observed NIR emission originates in the thermal emission of hot dust in the innermost dust torus.

According to the AGN unified model, one may expect that the emission from the innermost dust torus is totally obscured by the outer dust torus. However, high angular-resolution integral-field spectroscopies reported that some of type 2 AGNs follow the correlation for type 1 AGNs between the NIR luminosity and the isotropic luminosity indicators (such as mid-infrared continuum emission and hard X-ray emission). This correlation suggests that a significant amount of the NIR flux comes from hot dust in the innermost dust torus in relatively less obscured type-2 AGNs (Burtscher et al. 2015; Müller-Sánchez et al. 2019). Burtscher et al. (2015) reported that NGC 2110 is one of those less obscured type-2 AGNs, supported by its relatively small hydrogen column density of  $N_{\text{H}} \sim 5 \times 10^{22} \text{ cm}^{-2}$  (Marinucci et al. 2015; Baloković, et al. 2018). In fact even a Compton-thick (i.e. heavily-obscured) type-2 AGN, NGC 1068, was reported to show a large amplitude of NIR flux variations (Glass 2004; Taranova & Shenavrin 2006)<sup>3</sup>. Furthermore, a recent NIR interferometer observation of it found a ring-like structure of emission, which was associated with the dust sublimation region (GRAVITY Collaboration 2020). As such, observations of NGC 1068 revealed that even heavily-obscured type-2 AGNs, if not all of them, show NIR nucleus emission, which implies that NIR nucleus emission originating probably in the innermost dust torus may be common among any type 2 AGNs, let alone less obscured ones like NGC 2110. Therefore, it is likely that the observed NIR continuum emission and its flux variation of NGC 2110 originate in the innermost dust torus.

We have estimated the full widths of the TF to be approximately  $w_{W1} \sim 300$  days and  $w_{W2} \sim 330$  days for the W1 and W2 bands, respectively. Thus the TF is considerably extended. The width of the TF of the torus emission is generally larger when the viewing angle is larger (e.g., Barvainis 1992; Kawaguchi & Mori 2011; Almeyda et al. 2020). In general, type 2 AGNs are considered to have a large viewing angle according to the unified model; accordingly the TF of type 2 AGNs should be extended. Therefore, our estimated large width of the TF for NGC 2110 is consistent with the picture of the unified model.

We have used JAVELIN for the lag estimation, which assumes a top-hat function in the transfer equation, and have estimated the most likely time lag of  $\tau_{\text{dust}} \sim 130$  days and full width of  $w \sim 300$ – $330$  days for the TF. This TF has a positive value of the response lag from  $\sim -30$  days to  $\sim 290$  days; this means that the earliest NIR flux variation starts  $\sim 30$  days ( $\sim 10\%$  of the full width of the TF)

<sup>3</sup> Gallimore et al. (2001) explained the loss of the maser signal and the peak of the NIR light curve of NGC 1068 with reverberation of a suppositional flare of the nucleus emission.



before its triggering X-ray flux variation. This negative lag response apparently violates causality and therefore should not be real. We conjecture that it is caused by JAVELIN's assumption of the top-hat shape for the TF without any constraints between the lag and width in the calculation and also by the sparse monitoring sampling of the IR flux variations. Data from monitoring observations with a high cadence combined with methods of non-parametric reconstruction of the TF (e.g., Horne 1994; Pijpers & Wanders 1994; Krolik & Done 1995) will enable us to constrain the shape of the TF and provide more detailed information on the geometry and physical parameters of the innermost dust torus.

The dust reverberation mapping can be applied even to obscured AGNs, as we have demonstrated in this work. The viewing-angle dependence of the torus TF can be studied by a systematic dust reverberation survey on both type 1 and type 2 AGNs, which will resolve part of parameter degeneracy in the torus TF. Understanding the dust tori of AGNs is also important for investigating the radius-luminosity relation of AGNs, which is used as a high-redshift distance indicator (e.g., Yoshii et al. 2014; Hönig 2014; Koshida et al. 2017), because the relation might be affected by the dust torus parameters in each AGN (e.g., Yoshii et al. 2014; Minezaki et al. 2019). More systematic studies of type 2 AGNs are desired with simultaneous X-ray and NIR monitoring. For example, not only *MAXI* but also *Swift*/BAT data of type 2 AGNs are useful to be compared with NIR data including the *WISE* archive data. Our results will be reported in the forthcoming paper.

Another promising tool to investigate the torus structure is X-ray microcalorimeter spectroscopy of a narrow Fe-K $\alpha$  line, which will provide useful information on kinematics in the dust torus from its line width and profile, as demonstrated by the study of NGC 1275, using the Soft X-ray Spectrometer (SXS) on board the Hitomi satellite (Hitomi Collaboration 2018). The next X-ray microcalorimeter mission *XRISM* will be launched from Japan Aerospace Exploration Agency (JAXA) in 2021 Japanese fiscal year, and *Athena* is planned to be launched from European Space Agency (ESA) in 2031. With combination of the future X-ray microcalorimeter studies and the dust reverberation mappings on various types of AGNs, as well as IR interferometer observations, our understanding of the innermost torus will be dramatically improved.

## 5 CONCLUSIONS

We performed dust-reverberation mapping on the type 2 AGN NGC 2110 for the first time, using the 2–20 keV *MAXI* data and the W1- and W2-band *WISE* data. We conducted the ICCF analyses and JAVELIN simulations to compare them and obtained possible dust-reverberation time lags  $\tau_{\text{dust}}$  for both the W1 and W2 bands of  $\sim 60$  days,  $\sim 130$  days and  $\sim 1250$  days. We moreover examined the X-ray and IR best-fitting modelled light curves obtained by the JAVELIN runs. As a result, we revealed that the time lag of  $\tau_{\text{dust}} \sim 130$  days is most favoured. By employing the time lag of  $\tau_{\text{dust}} \sim 130$  days, the  $\tau_{\text{dust}}-L_{\text{bol}}$  relation of NGC 2110 was found to be consistent with those in type 1

AGNs. This means that the dust reverberation originates in hot dust around the innermost region of the dusty torus in the type-2 NGC 2110 as in the type 1 AGN. The present study demonstrated that X-ray and IR simultaneous monitoring is a powerful method to conduct dust-reverberation mapping on type 2 AGNs. To combine them with observations with future X-ray microcalorimeter missions will enable us to gain deeper insight about the innermost regions of AGN tori.

## ACKNOWLEDGEMENTS

We thank the anonymous referee for his/her valuable suggestions and comments. We are grateful for prof. Martin Ward for his helpful comments. We thank Dr. Nakahira for his useful comments about the *MAXI* data. This research has made use of *MAXI* data provided by RIKEN, JAXA and the *MAXI* team. This publication makes use of data products from the Wide-field Infrared Survey Explorer, which is a joint project of the University of California, Los Angeles, and the Jet Propulsion Laboratory/California Institute of Technology, funded by the National Aeronautics and Space Administration. This research is supported by Japan Society for the Promotion of Science (JSPS) KAKENHI with the Grant number of 16H02162, 17J09016, 19K21884, and 20H01947. Part of this research was financially supported with the Grant-in-Aid for JSPS Fellows for young researchers (T.K. and M.K.).

## REFERENCES

- Almeyda, T., Robinson, A., Richmond, M., Nikutta, R., and McDonough, B., 2020, *ApJ*, 891, 26  
 Antonucci, R. 1993, *ARA&A*, 31, 473  
 Baloković M., et al., 2018, *ApJ*, 854, 42  
 Barvainis R., 1987, *ApJ*, 320, 537  
 Barvainis R., 1992, *ApJ*, 400, 502  
 Baskin A., Laor A., 2018, *MNRAS*, 474, 1970  
 Burtscher, L. et al., 2015, *A&A*, 578, 47  
 Clavel, J., Wamsteker, W., and Glass, I. S., 1989, *ApJ*, 671, 124  
 Edelson, R., Gelbord, J. M., Horne, K., et al. 2015, *ApJ*, 806, 129  
 Edelson R., et al., 2017, *ApJ*, 840, 41  
 Gallimore, J. F., Henkel, C., Baum, S. A., et al. 2001, *ApJ*, 556, 694  
 Gardner E., Done C., 2017, *MNRAS*, 470, 3591  
 Glass, I. S., 2004, *MNRAS*, 350, 1049  
 GRAVITY Collaboration 2019, arXiv, arXiv:1910.00593  
 Gravity Collaboration 2020, *A&A*, 634, A1  
 Hitomi Collaboration, et al., 2018, *PASJ*, 70, 13  
 Hönig S. F., 2014, *ApJ*, 784, 4  
 Hönig S. F., Kishimoto M., 2017, *ApJL*, 838, L20  
 Horne, K., 1994, *ASP. Conference Series*, 69, 23  
 Huffman, D. R., 1977, *AdPhy*, 26, 129  
 Kawaguchi, T. and Mori, M., 2011, *ApJ*, 737, 105  
 Kawamuro T., Ueda Y., Tazaki F., Ricci C., Terashima Y., 2016, *ApJS*, 225, 14  
 Kawamuro T., et al., 2018, *ApJS*, 238, 32  
 Kelly, B. C., Bechtold, J., & Siemiginowska, A. 2009, *ApJ*, 698, 895  
 Kishimoto M., et al., 2011, *A&A*, 527, A121  
 Krolik J. H., Horne K., Kallman T. R., Malkan M. A., Edelson R. A., Kriss G. A., 1991, *ApJ*, 371, 541  
 Krolik, J. H., and Done, C., 1995, *ApJ*, 440, 166

- Koshida, S., Minezaki, T., Yoshii, Y., et al. 2014, *ApJ*, 788, 159  
 Koshida, S., Yoshii, Y., Kobayashi, Y., et al. 2017, *ApJ*, 842, 13  
 Koss M., et al., 2017, *ApJ*, 850, 74  
 Lebofsky, M. J. and Rieke, G. H., 1980, *Nature*, 284, 410  
 Lyu J., Rieke G. H., Shi Y., 2017, *ApJ*, 835, 257  
 Lyu J., Rieke G. H., Smith P. S., 2019, *ApJ*, 886, 33  
 Mainzer, A., Bauer, J., Cutri, R. M., et al. 2014, *ApJ*, 792, 30  
 Marinucci, A., Matt, G., Bianchi, S., et al. 2015, *MNRAS*, 447, 160  
 Matsuoka, M., Kawasaki, K., Ueno, S., et al. 2009, *PASJ*, 61, 999  
 Mehdipour M., et al., 2011, *A&A*, 534, A39  
 Mihara, T., Nakajima, M., Sugizaki, M., et al. 2011, *PASJ*, 63, S623  
 Minezaki T., Matsushita K., 2015, *ApJ*, 802, 98  
 Minezaki T., et al., 2019, *ApJ*, 886, 150  
 Miyake K., Noda H., Yamada S., Makishima K., Nakazawa K., 2016, *PASJ*, 68, S28  
 Müller-Sánchez, F., Hicks, E. K. S., Malkan, M., Davies, R., Yu, P. C., Shaver, S., & Davis, B., 2018, *ApJ*, 858, 48  
 Mor R., Netzer H., Elitzur M., 2009, *ApJ*, 705, 298  
 Noda H., Makishima K., Uehara Y., Yamada S., Nakazawa K., 2011, *PASJ*, 63, 449  
 Noda H., Makishima K., Yamada S., Torii S., Sakurai S., Nakazawa K., 2011, *PASJ*, 63, S925  
 Noda H., Makishima K., Nakazawa K., Uchiyama H., Yamada S., Sakurai S., 2013, *PASJ*, 65, 4  
 Noda H., Makishima K., Nakazawa K., Yamada S., 2013, *ApJ*, 771, 100  
 Noda H., Makishima K., Yamada S., Nakazawa K., Sakurai S., Miyake K., 2014, *ApJ*, 794, 2  
 Noda, H., Minezaki, T., Watanabe, M., et al. 2016, *ApJ*, 828, 78  
 Noda H., Done C., 2018, *MNRAS*, 480, 3898  
 Penston, M. V., Penston, M. J., Selmes, R. A., Becklin, E. E., & Neugebauer, G., 1974, *MNRAS*, 169, 357  
 Peterson B. M., Wanders I., Horne K., Collier S., Alexander T., Kaspi S., Maoz D., 1998, *PASP*, 110, 660  
 Petrucci P.-O., et al., 2018, *A&A*, 611, A59  
 Pijpers, F. P. and Wanders, I., 1994, *MNRAS*, 271, 183  
 Ricci C., et al., 2017, *ApJS*, 233, 17  
 Shappee, B. J., Prieto, J. L., Grupe, D., et al. 2014, *ApJ*, 788, 48  
 Salpeter, E. E., 1977, *ARA&A*, 15, 267  
 Storchi-Bergmann T., Winge C., Ward M. J., Wilson A. S., 1999, *MNRAS*, 304, 35  
 Suganuma, M., Yoshii, Y., Kobayashi, Y., Minezaki, T., Enya, K., Tomita, H., Aoki, T., Koshida, S., and Peterson, B. A., 2006, *ApJ*, 639, 46  
 Taranova, O. G. and Shenavrin, V. I., 2006, *A&AT*, 25, 233  
 Tomida, H., Tsunemi, H., Kimura, M., et al. 2011, *PASJ*, 63, 397  
 Urry, C. M., & Padovani, P. 1995, *PASP*, 107, 803  
 Vasudevan R. V., Fabian A. C., 2009, *MNRAS*, 392, 1124  
 Wright, E. L., Eisenhardt, P. R. M., Mainzer, A. K., et al. 2010, *AJ*, 140, 1868  
 Woo, J.-H., & Urry, C. M. 2002, *ApJ*, 579, 530  
 Yoshii, Y., Kobayashi, Y., Minezaki, T., Koshida, S., & Peterson, B. A. 2014, *ApJ*, 784, L11  
 Zu, Y., Kochanek, C. S., & Peterson, B. M. 2011, *ApJ*, 735, 80  
 Zu, Y., Kochanek, C. S., Kozłowski, S., & Udalski, A. 2013, *ApJ*, 765, 106

This paper has been typeset from a  $\text{\TeX}/\text{\LaTeX}$  file prepared by the author.